ELSEVIER

Journal of Nuclear Materials 296 (2001) 155–164

journal of nuclear materials

www.elsevier.com/locate/jnucmat

# Impact of irradiation on the tensile and fatigue properties of two titanium alloys

P. Marmy *, T. Leguey

*Centre de Recherche en Physique des Plasmas, Technologie de la Fusion, Association Euratom – Confédération Suisse, Ecole Polytechnique Fédérale de Lausanne, 5232 Villigen-PSI, Switzerland*

**Abstract**

The attachment of the first wall modules of the ITER FEAT fusion reactor is designed using flexible connectors made from titanium alloys. An assessment of the tensile and fatigue performance of two candidate alloys, a classical two phase Ti6Al4V alloy and a monophase α alloy Ti5Al2.5Sn, has been carried out using 590 MeV protons for the simulation of the fusion neutrons. The dose deposited was up to 0.3 dpa and the irradiation temperature was between 40°C and 350°C. The unirradiated tensile performances of both alloys are roughly identical. The radiation hardening is much stronger in the α + β alloy compared with the α alloy, and the ductility is correspondingly strongly reduced. A very fine precipitation observed by TEM in the primary and secondary α grains of the dual phase alloy seems to be the cause of the intense radiation hardening observed. Two different regimes have been observed in the behaviour of the cyclic stresses. At a high imposed strain, the softening is small in the Ti6Al4V and larger in the Ti5Al2.5Sn. At a low imposed strain, and for both alloys, cyclic softening occurs up to about 800 cycles, but then a transition occurs, after which a regime of cyclic hardening appears. This cyclic hardening disappears after irradiation. In both materials, and for all test conditions, the compressive stress of the hysteresis loop was found to be larger than the tensile stress. The stress asymmetry seems to be triggered by the plastic deformation. The fatigue resistance of the Ti5Al2.5Sn alloy is slightly better than that of the Ti6Al4V alloy. The irradiation did not significantly affect the fatigue performance of both alloys, except for high imposed strains, where a life reduction was observed in the case of the Ti6Al4V alloy. SEM micrographs showed that the fractures were transgranular and pseudo-brittle. © 2001 Elsevier Science B.V. All rights reserved.

## 1. Introduction

Titanium alloys have been used extensively in the aerospace industry due to their excellent general properties and a high strength-to-weight ratio. Titanium alloys also show high potential for satisfying low activation requirements, as required in today's new nuclear developments [1]. A low elastic modulus of about 120 000 MPa was also a crucial parameter for the selection of Ti6Al4V, an α + β alloy, and Ti5Al2.5Sn, an α alloy, as candidate materials for manufacturing the flexible connectors attaching the first wall modules of the ITER FEAT fusion reactor.

One of the concerns in using titanium alloys in a radiation environment is radiation damage in terms of loss of ductility and embrittlement. The data available is very sparse, but some relevant studies can be found; for example, Higashiguchi and Kayano [2] have irradiated pure titanium with fast neutrons at fluences up to $3 \times 10^{19}$ n/cm$^2$ and at a temperature of less than 150°C. Their tensile tests were carried out at temperatures between that of liquid nitrogen and 135°C. They showed that the ductility at liquid nitrogen temperature was enhanced by irradiation and did not decrease significantly at the higher test temperatures. The corresponding hardening increased by up to 100% of the initial flow stress of the relatively soft titanium studied. Kohyama et al. [3] irradiated pure Ti and Ti6Al4V with neutrons at

* Corresponding author. Tel.: +41-56 310 2932; fax: +41-56 310 4529.

*E-mail address:* pierre.marmy@psi.ch (P. Marmy).

0022-3115/01/$ - see front matter © 2001 Elsevier Science B.V. All rights reserved.
PII: S0022-3115(01)00564-5

fluences up to $5 \times 10^{20}$ n/cm$^2$ at 260°C. In pure Ti they observed a saturation of hardening at a fluence of $1.2 \times 10^{20}$ n/cm$^2$, and a hardening of approximately 35% of the initial flow stress. In the Ti6Al4V alloy, no saturation of hardening was observed, and the irradiation hardening and corresponding loss of ductility was more significant than in pure Ti.

Both candidate alloys have been irradiated with 590 MeV protons at the PSI accelerator in Villigen, Switzerland, in order to simulate 14 MeV fusion neutrons. The irradiation temperatures were between 40°C and 350°C and the dose reached up to 0.3 dpa, which corresponds with a good margin of error to the service dose limit of the flexible connectors in ITER. The unirradiated tensile and fatigue properties of both alloys have been described previously [4], where it was shown that both alloys had very similar tensile and fatigue properties, with the α alloy being slightly superior due to lower cyclic stresses. This paper describes the effects of the proton irradiation on the same properties, with the objective of assessing embrittlement at low strain rates. TEM and SEM microscopy was undertaken, to understand the observed effects on the mechanical properties.

## 2. Experimental

### 2.1. Materials, irradiation parameters and specimens

The Ti5Al2.5Sn alloy follows the AMS 4926H specification. After hot forming, it was annealed for 1 h at 815°C and then air cooled. The finished stock is a round bar of 31.75 mm diameter. The mill-annealed Ti6Al4V alloy was produced according to the specifications WL 3.7164.1 and DIN 65040/65174 to a stock diameter of 150 mm. It was annealed for 1.5 h at 730°C and then air cooled. The chemical specification of both alloys is given in Table 1.

The irradiation took place at the proton accelerator of the Paul Scherrer Institute, Villigen, Switzerland. The available beam had a maximal proton intensity of 20 μA and an energy of 590 MeV. This type of high-energy particle also produces the helium typical of fusion neutrons, alongside the displacement damage. The proton beam has a gaussian form and fluctuates with a frequency of 1 Hz over the specimen, to achieve a constant dose along the gauge length. In order to control the irradiation temperature, specimens have to be actively cooled in a flow of pressurised helium [5]. The dose was estimated from the beam-time integral and from dosimetry experiments using the Na22, Ti44 and Sc46 production isotopes. The mean parameters obtained during the titanium alloys experiments were:

| | |
|---|---|
| Irradiation temperature | 40°C, 200°C and 350°C |
| Mean proton flux | $1.2 \times 10^{15}$ p/cm$^2$ s |
| Mean dpa rate | $3 \times 10^{-6}$ dpa/s |
| Mean helium production rate | 50 appm/dpa |
| Accumulated dose | 0.01, 0.1, 0.2 and 0.3 dpa |

Testing was carried out using subsize specimens specially designed for the proton experiment, having a rectangular cross-section of $0.34 \times 4$ mm$^2$ for the tensile tests and a tubular cross-section of $3.4 \times 2.7$ mm$^2$ for the fatigue tests. Both specimens had a gauge length of 5.5 mm. Drawings of the specimens can be seen in [6].

### 2.2. Mechanical tests

Mechanical tests were performed using an RMC100 mechanical testing machine. Tests at elevated temperature (>RT) were performed in a vacuum furnace at a pressure near $10^{-6}$ mbar. Tensile testing compared the properties of the two alloys at a strain rate of $3 \times 10^{-4}$ s$^{-1}$. Fatigue tests were carried out at 350°C under total strain control ($R = -1$), at a strain rate between 0.001 and 0.002 s$^{-1}$. The strain was measured with an automatic strain extensometer, specially designed for testing radioactive specimens. The extensometer was regularly calibrated at the test temperature after the specimen had separated into two pieces, using a reference extensometer on the crosshead. The rupture criteria used to describe the fatigue life is that the specimen was considered to be ruptured when the first crack passed through the wall of the specimen (0.34 mm). This fracture criterion, called $N_a$, has a smaller statistical spread in the case of thin-wall specimens and corresponds to the appearance of an inflection point on the compressive region of the hysteresis loop.

### 2.3. Microstructural observations

The general microstructure was obtained from optical and scanning microscopy, using mainly polarised light on an unetched polished surface for the optical

Table 1
Chemical compositions [wt%]

| | Al | C | Fe | Sn | $H_2$ | $N_2$ | $O_2$ | V | Others |
|---|---|---|---|---|---|---|---|---|---|
| Ti5Al2.5Sn | 5.0 | 0.17 | 0.36 | 2.4 | 0.0036 | 0.010 | 0.179 | – | |
| Ti6Al4V | 6.08 | 0.0056 | 0.1399 | – | <0.0060 | 0.0065 | 0.176 | 3.95 | <0.4 |

microscopy. Fractographs were analysed with a Zeiss DSM 962 scanning electron microscope equipped with a tungsten cathode, operating at a maximum voltage of 30 keV. Transmission electron microscopy examinations were made on thin foils prepared by electropolishing using a solution of 3% perchloric acid, 37% 2-butoxyethanol and 60% ethanol at 20 V and −35°C, and examined in a JEOL 2010 operating at 200 kV.

## 3. Results

### 3.1. As-received microstructure

The Ti5Al2.5Sn alloy has a globular appearance with fine, equiaxial grains, mostly of the order of 20 μm in size. Another population of larger grains, of about 40 μm or more, also exists. Usually, the larger grains contain the smaller ones. This heterogeneity of the structure is more visible in micrographs taken along the material drawing axis. After etching with a solution of 10 ml HF, 40 ml $HNO_3$ and 50 ml $H_2O$, lines of preferential attack appear, extending along many grains. SEM observations identified these lines as a new phase having different distribution for transversal and longitudinal sections. EDS analysis indicated that the concentration of iron is higher in this phase than in the matrix. The total amount of this iron-rich phase was estimated to be ~1%. Diffraction electron microscopy confirmed the bcc structure of the retained phase.

The Ti6Al4V alloy has a globular structure, composed of primary grains of around 20 μm in size, and colonies of secondary elongated α grains, surrounded by the intergranular β phase. The volume fraction of the β phase is around 13%. Due to its different composition, the β phase is readily visible at the boundaries and appears as intergranular bands of 0.05–1 μm width. A detailed study of the microstructure of the unirradiated alloys can be found in [7].

### 3.2. Tensile tests of Ti5Al2.5Sn and Ti6Al4V alloys

In a previous article [4], it was reported that results obtained with the subsize PIREX specimen were validated by comparing them with a series of tests using a specimen of a standard geometry. The comparison proved to be satisfactory. It was also shown that both alloys had very similar tensile properties, with a yield stress at room temperature of approximately 800 MPa, a total elongation of 10–15% and a uniform elongation of 5–9% [4]. There was a yield point systematically present on the deformation curves of the α alloy, whereas the Ti6Al4V did not show one. Furthermore, the α alloy developed more dynamic strain aging in comparison with the α + β alloy. The effect of irradiation on the strain flow in the α material was such that the yield point was suppressed and the dynamic strain aging enhanced. No such effect occurred in the α + β alloy.

After annealing for 5 h at 750°C (heat treatment used to load hydrogen in titanium), it was found that the α + β alloy is more stable than the α alloy. The Ti6Al4V alloy did not show any change. The α alloy Ti5Al2.5Sn responded to the treatment by exhibiting reduced strength and improved ductility (−60 MPa on $\sigma_{0.2}$ and +3% on total elongation $\varepsilon_{tot}$, at 275°C).

For both alloys, the main effect of the irradiation was to increase the stress level and reduce the ductility. However, the effects were much stronger in the α + β alloy, as can be seen in Fig. 1, which shows the deformation curves obtained at room temperature after irradiation at 350°C to 0.3 dpa.

The amount of irradiation hardening observed in the Ti5Al2.5Sn irradiated at 350°C was small. The strength was also little affected by irradiation at 40°C, as can be seen in Fig. 2, but the ductility was reduced by about 15% after 0.01 dpa (Fig. 2).

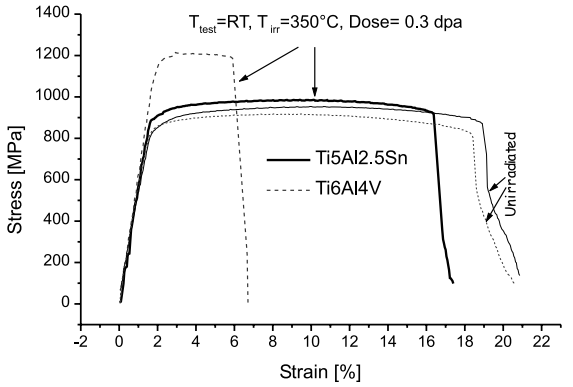


Fig. 1. Deformation curves before and after irradiation ($T_{irr}$ = 350°C/0.3 dpa) obtained at room temperature.

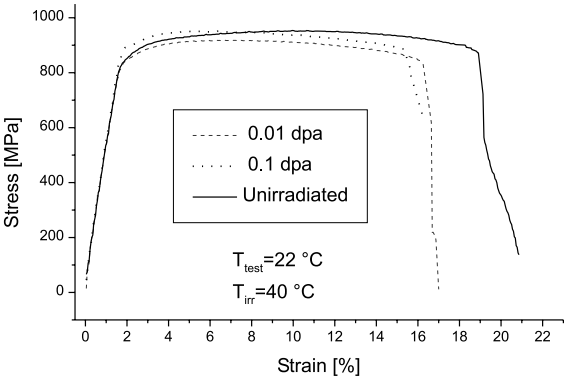


Fig. 2. Deformation curves of Ti5Al2.5Sn before and after irradiation at 40°C.

The behaviour of the yield and ultimate stresses before and after irradiation is indicated in Fig. 3, as a function of the test temperature. The high temperature irradiation influenced both the yield and ultimate stresses, and the measured irradiation hardening was independent of temperature. This behaviour is athermal in nature and the dislocation glide is affected by long-range obstacles. The low temperature irradiation (Fig. 3(c), Ti5Al2.5Sn) mainly affected the yield stress. The ultimate stress increased by only a few MPa's.

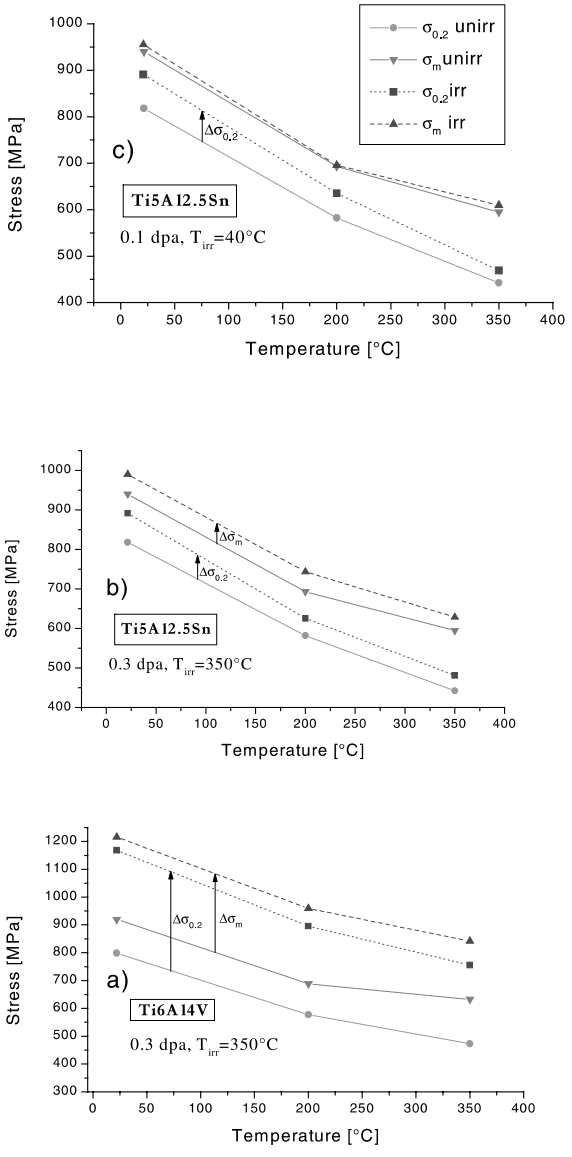


Fig. 3. The effect of irradiation on the yield and ultimate stresses as a function of test temperature: (a) Ti6Al4V, $T_{irr} = 350°C/0.3$ dpa; (b) Ti5Al2.5Sn, $T_{irr} = 350°C/0.3$ dpa; (c)Ti5Al2.5Sn, $T_{irr} = 40°C/0.1$ dpa.

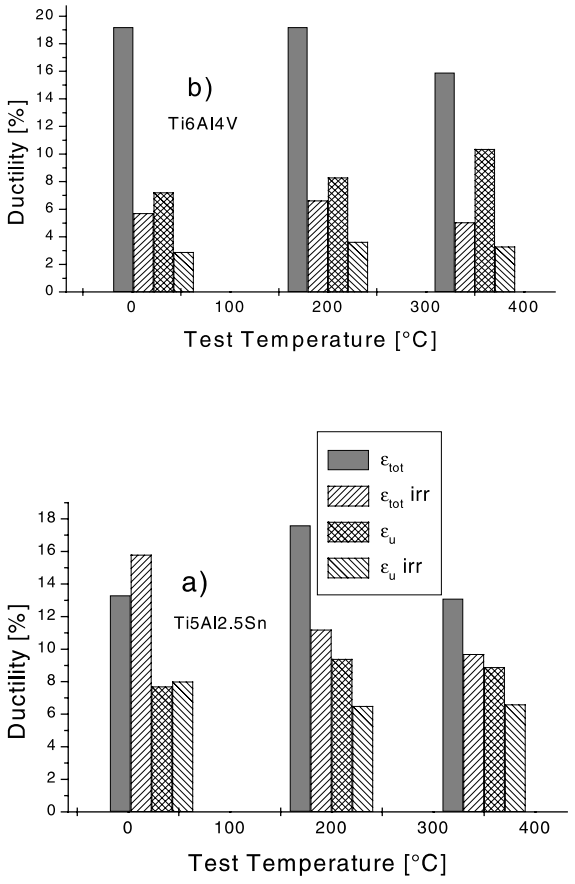


Fig. 4. The effect of irradiation ($T_{irr} = 350°C/0.3$ dpa) on the total elongation $\varepsilon_{tot}$ and uniform elongation $\varepsilon_u$ as a function of test temperature: (a) Ti5Al2.5Sn; (b) Ti6Al4V.

In Fig. 4, the behaviour of the uniform and total elongations is shown for both alloys, irradiated to 0.3 dpa at 350°C, as a function of test temperature. It can be clearly seen that the ductility of the $\alpha + \beta$ alloy was more strongly affected than that of the $\alpha$ alloy, especially when tested at room temperature.

The microstructure of the specimen irradiated to 0.3 dpa at 350°C and tensile tested to rupture at room temperature was examined in the TEM.

The Ti5Al2.5Sn alloy showed arrays of parallel dislocations resulting from the tensile testing, although not as extended as in the unirradiated case [7]. Irradiation damage appeared mainly in the form of black dots homogeneously distributed.

In the case of the Ti6Al4V alloy, no straight dislocations were visible in the $\alpha$ grains. There was a dense dislocation forest in the primary and secondary $\alpha$ grains. After achieving diffraction conditions of almost invisibility contrast for the dislocations, a fine precipitation could be observed (see Fig. 5(a)). Dark field images of

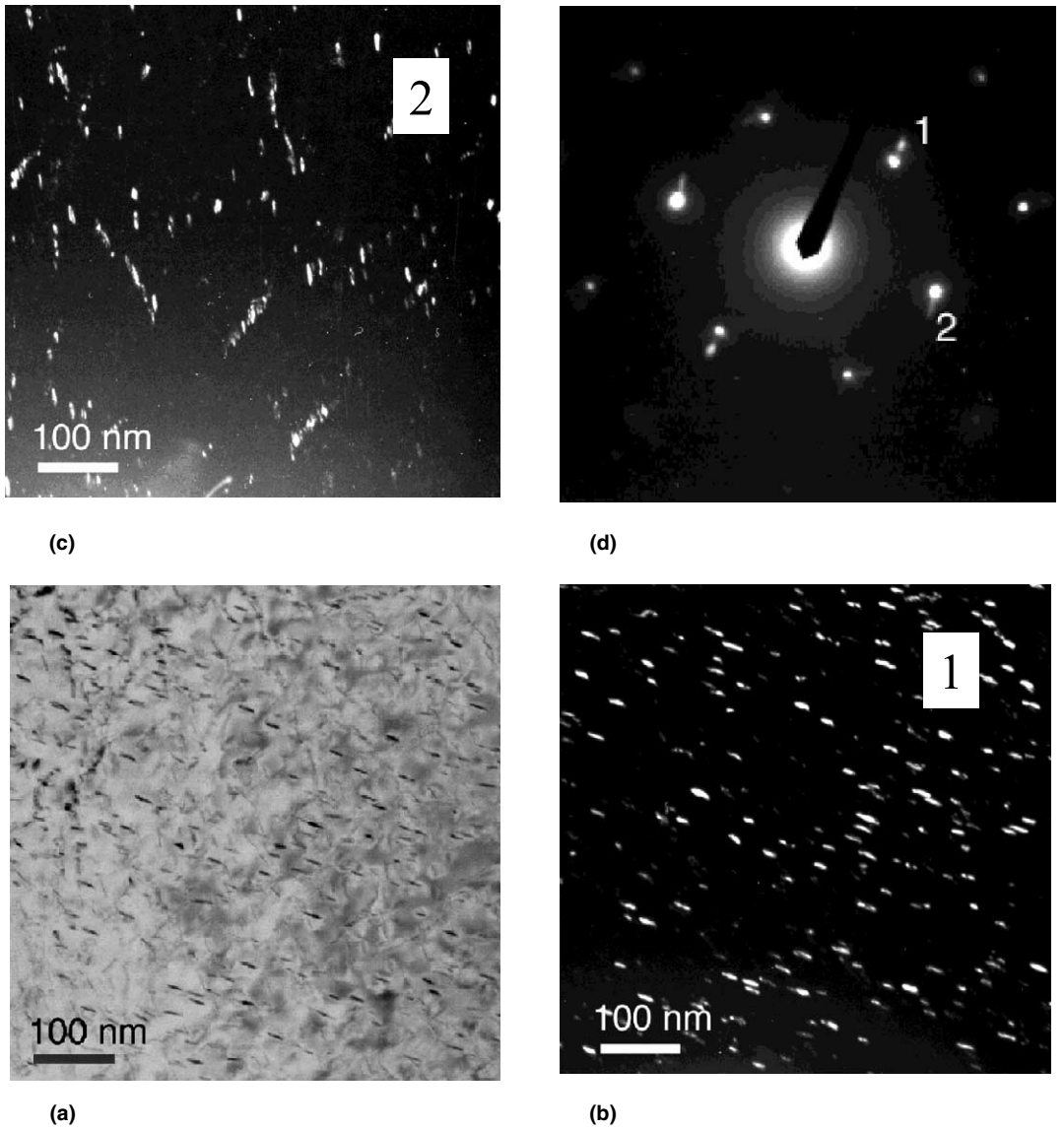


Fig. 5. Radiation-induced precipitation in the α phase of Ti6Al4V deformed at room temperature ($T_{irr} = 350°C/0.3$ dpa).

these precipitates are shown in Figs. 5(b) and (c), for two different diffraction spots (Fig. 5(d)). They are elongated particles of size up to 15 nm, with different orientations and distributions. Deformation-induced martensitic transformation also occurred in the β phase, as shown earlier for the unirradiated case [4,7].

### 3.3. Fatigue tests

The behaviour of the unirradiated alloys under fatigue testing has been reported previously in [4]. When these are tested at a medium imposed strain, up to about 800 cycles, both alloys initially show cyclic softening, with the softening being higher in the α alloy. Later, above 800 cycles, cyclic hardening is observed. This hardening may be due to the increasing density of dislocation residues produced during cyclic straining [4,7]. The cyclic hardening is higher in the α + β alloy than it is in the α alloy. In the Ti6Al4V, the stress at the end of life reaches the level it had at the first cycle. In the α alloy, the cyclic softening at half life increases slightly as the imposed strain increases. The softening is relatively important and is of the order of 80–100 MPa. In the α + β alloy, the softening at half life is absent at low imposed strains, but a value of 75 MPa was measured at 1.6%. The cyclic stresses are about 15% higher in the α + β alloy [4].

The cyclic softening behaviour of the irradiated material ($p = 0.3$ dpa; $T_{irr} = 350$°C) is shown in Fig. 6(a), for an imposed total strain of 1%. The secondary hardening disappeared in both materials after proton irradiation. The Ti5Al2.5Sn showed monotonic softening with increasing plasticity, whereas cyclic softening was absent in the Ti6Al4V alloy. This is because the stress was fully elastic, as can be seen from the very small, measured plastic strain range (Fig. 6(a)). Fig. 6(b) shows the softening behaviour for large imposed strains. Monotonic cyclic softening was observed in both materials. A continuously increasing plastic strain was now measured in the $\alpha + \beta$ alloy, this strain being a factor of three smaller than in the $\alpha$ alloy. The higher stress is caused by the higher irradiation hardening sensitivity of the $\alpha + \beta$ alloy, as shown in the preceding section.

Another general feature observed in the fatigue testing of both alloys, is the fact that the compressive stress of the hysteresis loop was always higher than the tensile stress [4]. Three examples of that asymmetry are shown in Fig. 7(a) for the unirradiated material. To help clarify the responsible mechanism, the stress asymmetry has been plotted as a function of the plastic strain range

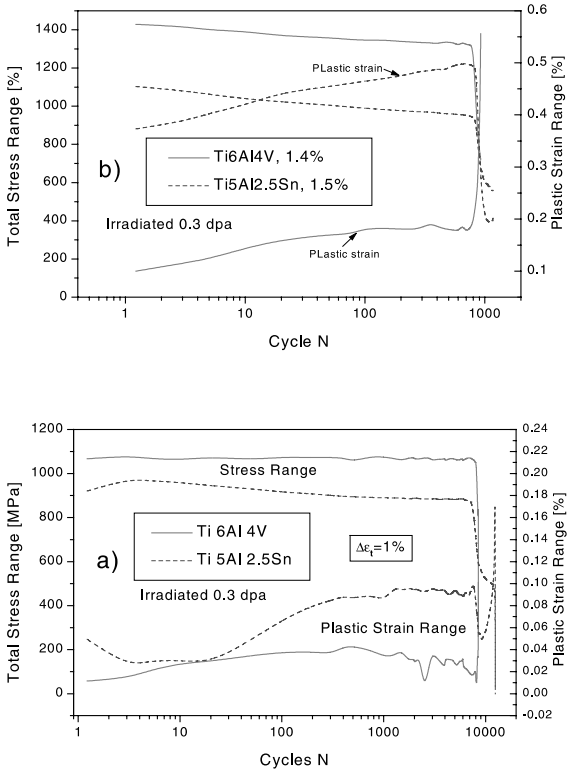


Fig. 6. The total stress range and plastic strain range as a function of cycle number for a low imposed total strain (a) and for a high imposed total strain (b), for the irradiated alloys ($T_{irr} = 350$°C/0.3 dpa).

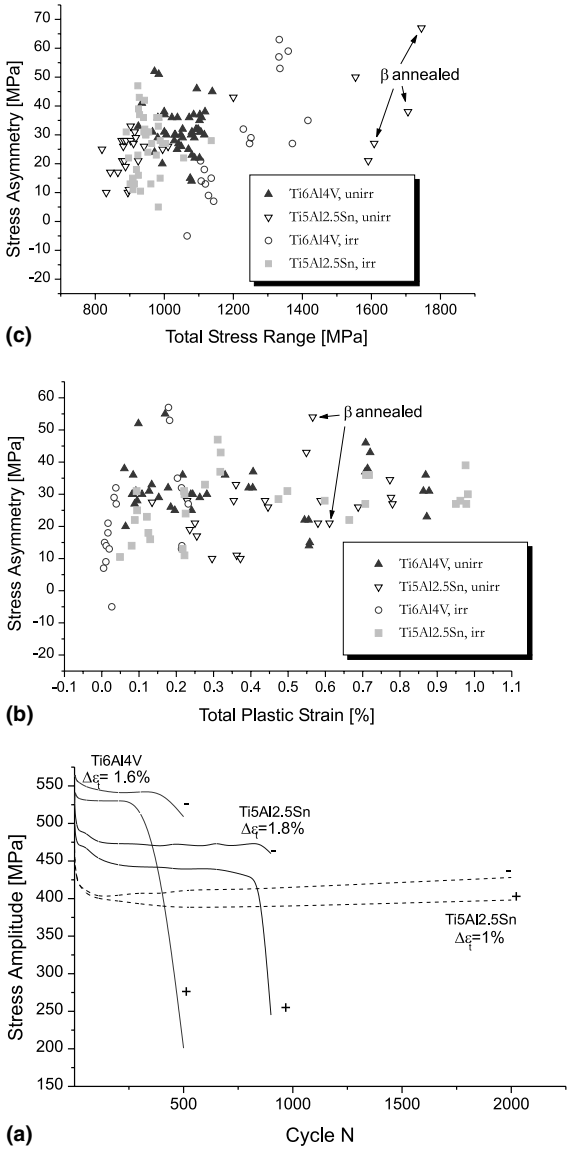


Fig. 7. (a) Compressive (−) and tensile (+) stress amplitude as a function of cycle number for different conditions. Cyclic stress asymmetry as a function of the total plastic strain (b) and total stress range (c) for the unirradiated and irradiated alloys ($T_{irr} = 350$°C/0.3 dpa). $T_{test} = 350$°C except for the beta annealed specimen tested at RT.

and total stress range in Figs. 7(b) and (c), for all conditions. No simple dependence can be found and the Figures indicate rather that the asymmetry seems to be triggered by the plastic strain and increases slightly as the total stress range increases.

The endurance of both alloys at 350°C has earlier been compared in the unirradiated condition for both alloys (see [4]). The low cycle fatigue resistance of the $\alpha$ alloy was found to be slightly higher. The comparison

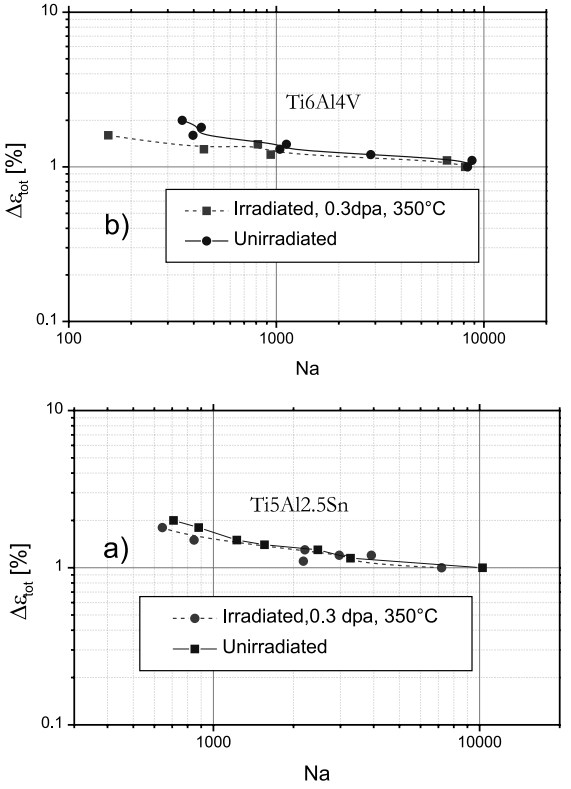


Fig. 8. The effect of irradiation ($T_{irr} = 350°C/0.3$ dpa) on the fatigue life of Ti5Al2.5Sn (a) and Ti6Al4V (b).

before and after irradiation at 350°C is shown for both alloys in Fig. 8. As shown by the log–log plot, there is no significative degradation of the fatigue life of the Ti5Al2.5Sn alloy. In the case of Ti6Al4V, and when the imposed total strain was above 1.2%, the lifetime was clearly reduced by the 0.3 dpa/350°C irradiation.

There is a single result from irradiation at 200°C to 0.2 dpa. At an imposed total strain of 1.6%, the lifetime was reduced by 21% ($N_a$ unirradiated = 1848). The mean cyclic softening rate was enhanced by the irradiation to a value of $1.79 \times 10^{-1}$ MPa/cycle (+24%). The $\sigma_{0.2}$ stress was measured at the first cycle (strain rate = 0.002 $s^{-1}$), and a value of $\Delta\sigma_{0.2} = 93$ MPa was derived for the irradiation hardening.

Fractographs of unirradiated and irradiated specimens were observed in the SEM. Generally, for both conditions and alloys, the rupture surfaces can be described as being transgranular and pseudo-brittle. There is a high density of secondary microcracks, with sizes between 2 and 50 μm, some of them placed between the grains (Fig. 9(a)). The majority of the surface is covered with cleavage facets with ductile edges. These facets are not pure cleaved surfaces because sometimes striations are visible on their surface, or near them at high magnification. Holes with sizes corresponding to the iron-rich particles observed in TEM, have been regularly found in the Ti5Al2.5Sn specimen (Fig. 9(b)). In Ti6Al4V, transcrystalline rupture was observed over small portions of the fractograph (Fig. 9(c)). No inclusions were seen on the fractographs of both alloys. Both alloys showed zones of localised deformation adjacent to zones that apparently seem very brittle. This is demonstrated in Fig. 9(d), where the bottom grain has striations and is separated from the adjacent grain by a crack.

## 4. Discussion

It is not surprising to have seen the iron-rich precipitates in the Ti5Al2.5Sn alloy, both after optical microscopy and TEM, because of the high iron concentration in the alloy (see Table 1). In fact, the solubility of Fe in the α phase of Ti is quite low and does not exceed 100 wppm at RT, as shown in the Ti–Fe phase diagram published by Kubatscheski et al. [8]. Above the solubility limit, a new phase, TiFe, is formed and segregates into the α phase.

Hardening produced by irradiation depends on the type and energy of the irradiating particle and also on the structure and chemical composition of the material irradiated. The irradiation hardening produced on the flow stress in the α alloy reached the values indicated in Table 2 for selected proton irradiation and test parameters. In this parameter range, the figures of Table 2 do not indicate a saturation of hardening. The greatest hardening is obtained for $T_{irr} = 200°C/0.2$ dpa. At $T_{irr} = 350°C$, the irradiation hardening rate is roughly a third of the value at $T_{irr} = 40°C$. There are no data available on irradiated Ti5Al2.5Sn. Hardening in pure Ti seems to be much higher at similar irradiation and testing conditions, as shown by Higashiguchi et al. and

Table 2
Irradiation hardening from 590 MeV protons in Ti5Al2.5Sn

| Test and irradiation parameters | $T_{test} = 22°C$, $T_{irr} = 40°C$, $D = 0.01$ dpa | $T_{test} = 200°C$, $T_{irr} = 40°C$, $D = 0.1$ dpa | $T_{test} = 200°C$, $T_{irr} = 200°C$, $D = 0.2$ dpa | $T_{test} = 200°C$, $T_{irr} = 350°C$, $D = 0.3$ dpa |
|---|---|---|---|---|
| $\Delta\sigma_{0.2,Irr}$ [MPa] | 19 | 55 | 93 | 46 |
| $\Delta\sigma_{0.2,Irr}$ [%] | +2.5 | +9.5 | +16 | +8 |

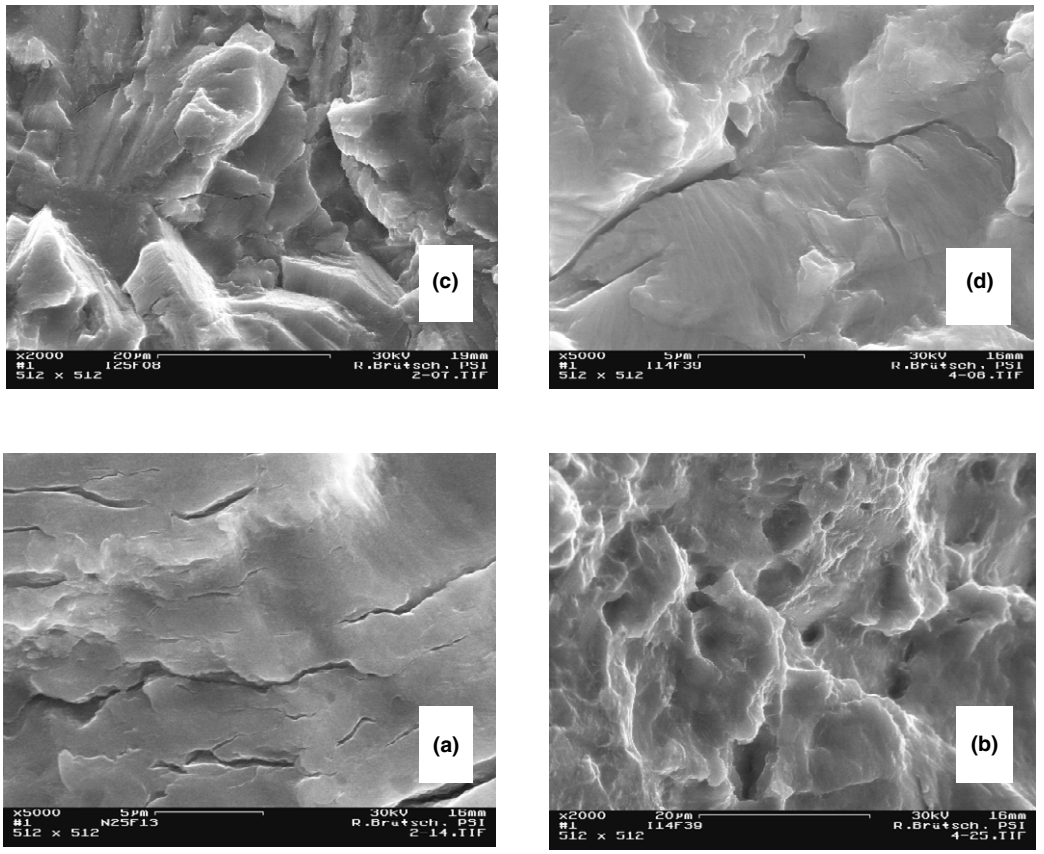


Fig. 9. Fractographs of fatigue specimens: (a) microcracks in unirradiated Ti6Al4V, $\Delta\varepsilon_t = 1.4\%$, $N_a = 1118$; (b) TiFe cavities and cleavage facets in irradiated Ti5Al2.5Sn ($T_{irr} = 350°C/0.3$ dpa), $\Delta\varepsilon_t = 1.5\%$, $N_a = 846$; (c) intergranular fracture in unirradiated Ti6Al4V, $\Delta\varepsilon_t = 1.4\%$, $N_a = 1118$; (d) crack separating a plastically deformed grain with striations from adjacent cleaved grains in irradiated Ti5Al2.5Sn ($T_{irr} = 350°C/0.3$ dpa), $\Delta\varepsilon_t = 1.5\%$, $N_a = 846$.

Kohyama et al. [2,3]. The weaker irradiation hardening of the alloy is due to the aluminum present (at 5%) in the α phase and to its ability to stabilise it, as demonstrated by Kojevnikov and Fabritsiev [9] for an accumulated dose of approximately 0.1 dpa (n) and irradiation temperature of 50–70°C.

In Ti6Al4V, the increase of the ultimate stress at room temperature induced by the protons ($T_{irr} = 350°C/0.3$ dpa) reached 300 MPa. Greater hardening, of approximately 500 MPa, was measured in the same alloy by Kohyama et al. [3], with neutrons ($T_{irr} = 260°C/0.3$–$0.5$ dpa). They identified the damage to be fine radiation-induced β phase precipitates and interstitial-type dislocation loops. The observed radiation hardening could be explained by a model based on dispersed obstacles. This is in accordance with the athermal behaviour shown in Fig. 3. The obstacles to dislocation motion are therefore strong and have a long-range stress field.

The presence of a β precipitation was also demonstrated by Plumton et al. [10], after irradiation with 9 MeV Al ions at temperatures between 500°C and 700°C. Their results showed that the precipitate size is inversely proportional to the irradiation temperature (between 65 and 400 nm). Furthermore, the results of Kojevnikov and Fabritsiev [9] indicated that increased hardening is the direct consequence of the presence of vanadium in the alloy. At a constant neutron fluence, the hardening increased linearly with vanadium content up to about 2%. Above this value, which corresponds to the maximum solubility of V in the α phase [8,9], saturation of irradiation hardening was observed.

The behaviour of both alloys is controlled by the irradiation response of their main component, the α phase. Therefore, the large difference in the behaviour after irradiation of both alloys is due to the beneficial effect of the Al in the Ti5Al2.5Sn alloy, and to the detrimental effect of V in the Ti6Al4V, which induces the precipitation of the very fine β particles.

As shown in Fig. 3(c) for the Ti5Al2.5Sn alloy, low temperature irradiation affects primarily the yield stress, and not the ultimate stress. This can be related to an

apparent strong reduction of the strain hardening capability, probably due to reduced dislocation mobility. This is consistent with the observed reduction of ductility after irradiation (Fig. 2).

The enhancement of dynamic strain aging in the irradiated Ti5Al2.5Sn specimen seems to indicate that irradiation promotes stress concentrations in this alloy. In fact, stress localisation helps to trigger flow instabilities.

The asymmetry of the flow stress in fatigue seems to be typical for titanium alloys (see also [11]), since it was observed in both alloys, and at all the test conditions applied in this study, including the irradiated condition. The asymmetry does not depend on the direction of the first cycle, whether it is a tensile or compressive stroke [11]. Therefore we can conclude that the asymmetry is caused by a different material behavior under positive or negative strain. It is difficult to discover the reason for this asymmetry. Many different mechanisms could be invoked, such as dislocation separation into partials and recombination processes, or different slip systems in the tensile and compressive regions. A more simple explanation could be that, due to the very marked texture of titanium alloys, large quantities of elastic energy are stored in the bulk and released during the tensile cycle. In fact, all fatigue specimens were cut along the longitudinal axis of the stock material. Fig. 7(b) shows that the asymmetry has survived β annealing (1/2 h 1055°C, AC, 1 h, 700°C, AC). Since the material was heated above the β transition, the heat treatment is supposed to have removed most of the texture, although this was not measured. Fig. 7(b) also shows that the magnitude of the asymmetry is independent of the amount of plastic strain, which does not support an explanation based on a dislocation mechanism.

According to the results presented above, the fatigue behaviour of both alloys appears to be very similar and not significantly affected by the irradiation. The small reduction in fatigue life (20–50%) after irradiation seems to be related to the increase in the stress level, especially at high strains, where higher stress concentrations occur. Brittle features, such as river patterns on cleaved facets, microcracks and small intergranular cracks, are observed in both materials in the unirradiated condition. The amount of these brittle features increases in the irradiated specimen, which is consistent with the measured reduction of the fatigue life. Partial intergranular fracture (Fig. 9(c)) could only be observed in the $\alpha + \beta$ alloy, thus indicating that it is slightly more brittle than the α alloy, in accordance with the observed lower life performance [4]. The specimen which failed suddenly at high strain (Fig. 8(b)) showed a transgranular and pseudo-ductile fracture, thus indicating that the failure was the result of a local instability (thin-wall specimen at cyclic stresses $>1500$ MPa) and not to brittleness. The key for understanding the general fatigue behaviour of these alloys, irradiated and unirradiated, is probably given in Fig. 9(d). There we see a well-deformed grain with striations at the surface that is adjacent to another grain that apparently failed through cleavage. Both are separated by a crack. The deformation in Ti is anisotropic, because it occurs mainly on the prismatic and pyramidal planes of the hcp lattice. The well-oriented grains deform plastically, but their neighbours cannot. The slip bands operative in the α grains are arrested at the grain boundaries because the boundaries are strength barriers but also because of the strain incompatibility between the adjacent grains with different orientation [12]. The localised plastic strain at the boundary has to be compensated for by corresponding elastic strains in the adjacent grains, which then induce an intense elastic field. The important dislocation activity at the boundaries produces dislocation residues and many point defects through dislocation intersection processes. These dislocation residues have been observed in the α grains and are thought to be responsible for the secondary cyclic hardening, as shown in [4]. Because the boundaries are strong sinks for point defects, the vacancies and residues which are produce by this mechanism can agglomerate and produce micro-voids. The growth of the micro-voids into larger voids by coalescence or micro-decohesions at the boundary is the mechanism creating an unrecoverable strain and nucleating the cracks. The energy for the growth process is provided by the huge elastic stress field. This process is biased by the stress, because it is much more effective under tensile strain. The specimen is forced externally to be extended by a certain distance, as commanded by the imposed strain signal. Some of this distance is provided freely, by the unrecoverable elongation. In fact, the specimen has been extended in the process, but it gets shortened on the subsequent reverse loading because the extensometer requires a longer travel back. This again contributes to a higher compressive stress and thus to the final stress asymmetry. Unlike a plastic material, where the plasticity would rapidly balance the stress, the pseudo-elastic material will balance it only slowly. A few cycles later, some more cracking occurs and the asymmetry is again reinforced. Once the micro-cracks have been nucleated, some will grow faster while other will be arrested, depending on their orientation. This nucleation process finally leads to the formation of a very high density of cracks (see Fig. 9(a)).

A similar mechanism has been proposed by Gilmore, 1976 [13], to explain the axial elongation of a Ti6Al4V specimen loaded under twist fatigue. It should be also noted that the transgranular nature of the cracks (only a minority are intergranular) is not in contradiction to the fact that the cracks initiate at the boundary. This is shown in [12]. Not all the unrecoverable strain is produced at the boundaries, much can be produced at other locations and does not contribute to the asymmetry.

The mechanism described above is probably the main mechanism available for the nucleation of a crack and its subsequent growth. It is common in both alloys, thus explaining their similar fatigue behaviour.

## 5. Summary of main results and conclusions

- The tensile strengths of the unirradiated alloys are very similar. The $\alpha + \beta$ structure is more stable and more highly resistant to heat treatment of 5 h/750°C. In Ti5Al2.5Sn, the yield point was eliminated and DSA slightly enhanced by irradiation. The radiation hardening on $\sigma_{0.2}$ is much greater in the $\alpha + \beta$ alloy than in the $\alpha$ alloy (369 MPa compared with 73 MPa at RT). Consequently, loss of ductility is more pronounced in the $\alpha + \beta$ alloy. Irradiation hardening is athermal and long-range in nature. In the $\alpha$ alloy, low temperature irradiation reduces the strain hardening performance. The different radiation hardening observed in the alloys can be explained by their different chemical composition.
- The Ti5Al2.5Sn contains a fine precipitation of Fe-rich precipitates. The microstructure after irradiation and tensile deformation in Ti5Al2.5Sn is characterised by black-dot defects and parallel dislocation arrays. In the Ti6Al4V, a fine radiation induced precipitation and a very high dislocation density are observed. Martensite is induced by strain in the $\beta$ phase.
- Typical cyclic stress behaviour was observed in both alloys, a softening regime at low cycles followed by a hardening regime at high cycles. The softening is higher in the $\alpha$ alloy. The hardening regime is absent in the irradiated specimen. Cyclic stresses are generally higher in the system $\alpha + \beta$. A cyclic stress asymmetry has been found for all testing conditions in both materials. The asymmetry occurs when plastic deformation is effective and seems to be caused by grain boundary micro-decohesions. For the irradiated and unirradiated condition, the fatigue endurance performance is slightly superior in the Ti5Al2.5Sn compared with the $\alpha + \beta$ alloy. Fractographs of both material indicate pseudo-brittle fracture. The strain appears to be localised in some well-oriented grains, but brittle fracture also occurs. The anisotropy of the material induces many small intra- and transgranular cracks. Crack nucleation mechanism is common in both materials, thus explaining their similar fatigue behaviour.

## Acknowledgements

The present work is partially funded by the European Fusion Technology Materials Program. We also thank the Paul Scherrer Institute at Villigen/CH for its support throughout this work, and we especially wish to express our thanks to R. Brütsch for performing the SEM observations of the fractographs.

## References

[1] J.W. Davis, M.A. Ulrickson, R.A. Causey, J. Nucl. Mater. 212–215 (1994) 813.
[2] Y. Higashiguchi, H. Kayano, J. Nucl. Sci. Technol. 12 (5) (1975) 320.
[3] A. Kohyama, K. Asano, N. Igata, J. Nucl. Mater. 141–143 (1986) 987.
[4] P. Marmy, T. Leguey, I. Belianov, M. Victoria, J. Nucl. Mater. 283–287 (2000) 602.
[5] P. Marmy et al., Nucl. Instrum. and Meth. B 47 (1990) 37.
[6] P. Marmy, R. Yuzhen, M. Victoria, J. Nucl. Mater. 179–181 (1991) 697.
[7] T. Leguey, R. Schablin, P. Marmy, M. Victoria, to be published.
[8] O. Kubaschewski, O. Kubaschewski-von Goldbeck, P. Rogl, H.P. Franzen, Atomic Energy Review, Titanium: Physico-Chemical Properties of its Compound and Alloys, Special Issue No. 9, Vienna, 1983.
[9] O.A. Kojevnikov, S.A. Fabritsiev, Vopr. Atom. Nayki Techn.; Fis. Radiaz. Povr. Radiaz. Material. 2 (44) (1988) 1.
[10] D.L. Plumton, G.L. Kulcinski, R.A. Dodd, J. Nucl. Mater. 144 (1987) 264.
[11] A.S. Beranger, X. Feaugas, M. Clavel, Mater. Sci. Eng. A 172 (1993) 31.
[12] K. Takao, K. Kusukawa, Mater. Sci. Eng. A 213 (1996) 81.
[13] C.M. Gilmore, M. Freedam, M.A. Imam, Mater. Sci. Eng. 8 (1976) 9.